Observations of the D and E mesons and possible three-kaon enhancements in $\pi^- p \to K^0 K^\pm \pi^\mp X$, $K^0 K^+ K^- X$ at 50 and 100 GeV/c

C. Bromberg,* J. O. Dickey, G. Fox, R. Gomez, W. Kropac,† J. Pine, and S. R. Stampke
California Institute of Technology, Pasadena, California 91125

H. Haggerty and E. Malamud
Fermi National Accelerator Laboratory, Batavia, Illinois 60510

R. Abrams, R. Delzenero, H. Goldberg, F. Lopez, S. Margulies, D. McLeod, and J. Solomon
University of Illinois at Chicago Circle, Chicago, Illinois 60680

A. Dzierba, F. Fredericksen, R. Heinz, J. Krider, H. Martin, and D. Petersen
Indiana University, Bloomington, Indiana 47401
(Received 14 April 1980)

We present results from the study of multikaon final states in the reactions $\pi^- p \to K^0 K^\pm \pi^\mp \tilde{X}$, $K^0 K^+ K^- \tilde{X}$ at 50 and 100 GeV/c. Here $\tilde{X}$ is semi-inclusive, that is, a specific forward topology and an interaction registering in the counters surrounding the target are required. The $D(1285)$ meson is seen in the $\delta\pi$ mode, while the $E(1420)$ meson is observed in both the $\delta\pi$ and the K^*K modes. In addition, there are two possible enhancements in the three-kaon final state. The first ($M \sim 1840$ MeV) is associated with the $K^0\phi$ mode and is consistent with being the charmed D^0. The second, a K^* state ($M = 2003 \pm 14$ MeV, $\Gamma = 87 \pm 43$ MeV), decays into KA_2.

I. INTRODUCTION

Results are presented from the study of multikaon final states in the reactions $\pi^- p \to K^0 K^\pm \pi^\mp \tilde{X}$, $K^0 K^+ K^- \tilde{X}$, where $\tilde{X}$ indicates a semi-inclusive trigger. The data are from the experiment E110 using the Fermilab multiparticle spectrometer in the M6W beam line with beam momenta of 50 and 100 GeV/c. The trigger was designed to select events with a neutral vee (decaying into two forward charged particles) plus two charged particles that trace back to an interaction vertex. In addition, a recoil registering in the counters surrounding the target is required. The identification of the outgoing charged particles is done using two Čerenkov counters.

High-energy (50 and 100 GeV/c) results on both $D(1285)$ and $E(1420)$ meson production are presented here. The D meson and the less studied E meson have been observed in many lower-energy experiments (see Particle Data Group[1] and recent papers[2-4]).

Some exciting physics are indicated in low-statistics three-kaon results where two possible mass enhancements are seen. Because of the kinematics ($M_{\text{resonance}} \gtrsim 3 M_K$), this is a particularly good channel for studying high-mass strange states. The first of these enhancements ($M = 1842 \pm 9$ MeV), associated with a $K^0\phi$ decay model, is consistent with being the charmed D^0. Its observed width (35 ± 30 MeV) agrees with the resolution of the spectrometer for this final state and has a semi-inclusive cross section times branching ratio of 0.05 ± 0.02 μb. The second enhancement, a K^* state ($M = 2003 \pm 14$ MeV, $\Gamma = 87 \pm 43$ MeV), decays into KA_2 and has a semi-inclusive cross section times branching ratio of 12 ± 2 μb.

In Sec. II we describe the experimental apparatus, event reconstruction, and Čerenkov identification system. In Sec. III the $K^0 K^\pm \pi^\mp$ final-state results, and evidence for the D and E mesons are presented. The three-kaon final state and its two possible mass enhancements are discussed in Sec. IV. The determination of cross sections times branching ratios is summarized in Sec. V and a conclusion is given in Sec. VI.

II. APPARATUS

A. Overview

The results presented here are from a data run of the Fermilab multiparticle spectrometer (MPS), which is shown in Figs. 1 and 2. Details of the spectrometer, beam, and track-finding algorithms are contained in unpublished reports.[5] A brief description of the apparatus will be presented. The event reconstruction and mass identification[6] of the outgoing particle will be discussed, since these procedures are central to the data analysis in this study.

The Fermilab MPS (Figs. 1 and 2) is designed to measure forward-going charged-particle systems. The spectrometer consists of a target and associated counters, proportional wire chambers (PWC's) and spark-chamber systems to detect and track charged particles, and two multicelled

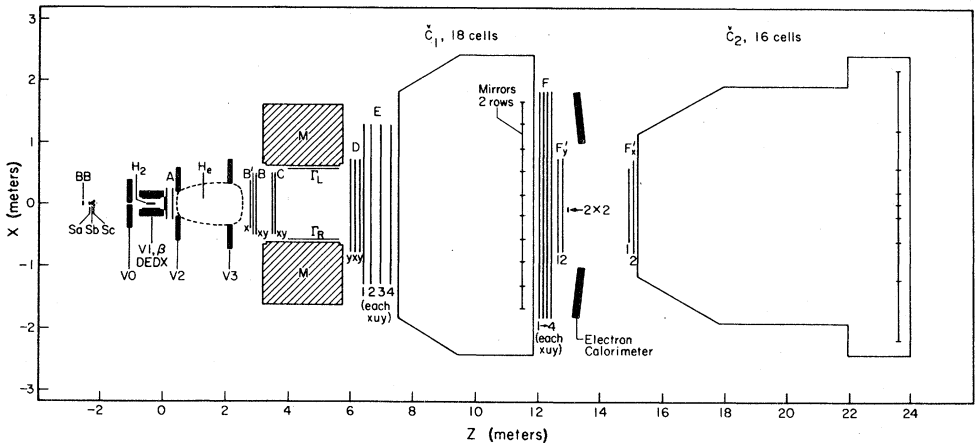

FIG. 1. Multiparticle spectrometer, plan view.

threshold Čerenkov counters. A large-aperture superconducting magnet (an iron "window-frame" magnetic design) is used for momentum analysis. The central field was operated at the maximum of 17.8 kG over an effective length of 1.4 m, imparting a transverse momentum of 0.75 GeV/c.

The M6W secondary beam to the MPS was operated both at 50 GeV/c (7% of the data) and 100 GeV/c (93% of the data). Four Čerenkov counters in the beam allowed for pion-kaon-proton tagging. A requirement of the data reported on here was that the beam particle be identified as a π. The direction of the beam was defined by proportional wire chambers (two planes of horizontal wires and two planes of vertical wires, all with a 2-mm pitch) located 19.7 m and three 1-mm pitch chambers (one plane each of horizontal, vertical, and slant wires) 2.2 m upstream of the target. The target region had a 12.0-in. liquid hydrogen target with a low-mass vacuum jacket, a cylindrical proportional wire chamber to detect charged particles coming from the recoiling target system, and a cylindrical shower counter. Two Čerenkov counters (C_1 and C_2) were used to identify the forward-going particles.

The trigger discussed here selects topology of vee plus two charged particles which trace back to the interaction vertex. The trigger was designed to be both strict enough to get a high K^0 yield and yet loose enough to allow for PWC inefficiencies and extra hits in the PWC's. Forward-multiplicity requirements for the trigger were made by counting hits in the proportional chambers in front of (stations A, B, C) and immediately behind (station D) the spectrometer magnet. These multiplicity requirements were two hits in two of

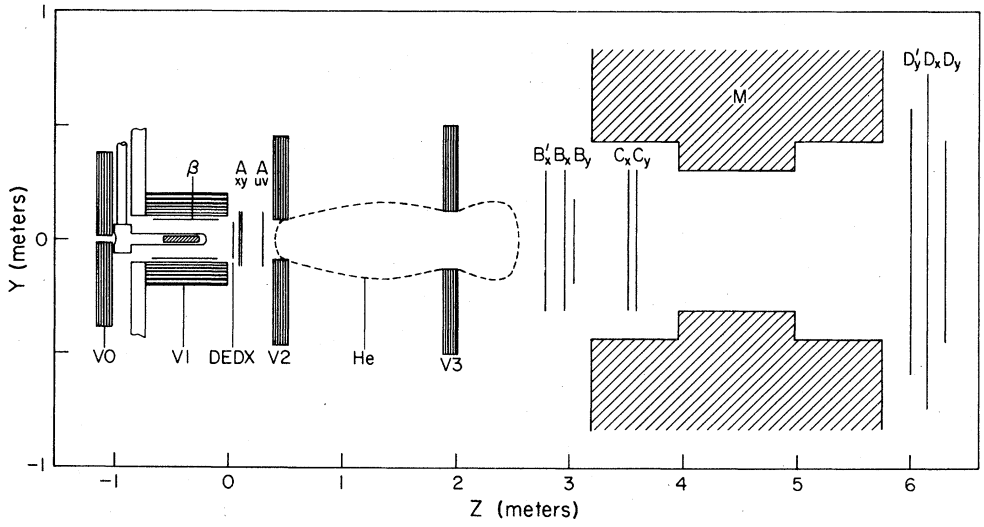

FIG. 2. Front-end side view of the multiparticle spectrometer.

three A chambers (A_x, A_y, A_u), exactly four hits in three of the six BCD chambers ($B_x, B_y, C_x, C_y, D_x, D_y$), three to five hits in five out of the six BCD chambers, and less than five hits in one of the two D chambers (D_x, D_y). Thus a vee was detected by a change in multiplicity in the decay region between the A and B stations.

The trigger also required less than three particles in a dE/dx counter about 25 cm downstream of the target to suppress unresolved particles at the A station. Finally, an interaction in the target was demanded by requiring at least one hit in either the cylindrical proportional wire chamber surrounding the target, or in a segmented cylindrical lead-scintillator sandwich counter surrounding the target and the cylindrical proportional wire chamber. The track-finding program (E110 TEARS, running on the CDC 7600 computer at LBL) reconstructed main and vee vertices and selected the best fit to the hypothesis of two forward-going charged particles from the interaction vertex and one vee projecting back to the interaction vertex.

B. Event reconstruction

The pattern recognition and event reconstruction for the vee- (V) plus-two-charged-particles triggers discussed here utilized much of the software developed for the Fermilab (E260) high-transverse-momentum experiment.[7] Modifications were made to improve the efficiency and background levels in events with low multiplicities, strange-particle decays, or high-momentum tracks near the beam line.

Reconstruction began downstream of the magnet where a track search was made independently in the x (11 planes) and y (12 planes) views. Matches between the x and y tracks were constructed by use of the 5.7°-stereo (8 planes) views. The minimal requirements placed on tracks and the high efficiency of the chambers indicate that only small individual track losses existed downstream of the magnet (apart from multiple scattering and secondary interactions in the spectrometer material). An attempt was then made to link, through the magnetic field, each matched track to the chamber hit patterns upstream of the magnet. This was done twice for each match: (1) using only the chambers which followed the strange-particle decay region (V-track candidates) and (2) using all the chambers downstream of the H_2 target (main vertex track candidates).

Reconstruction of V's was accomplished by looping over all V-track candidate pairs of opposite charge and attempting a vertex fit. The momentum vector of each V candidate with an acceptable χ^2 and vertex located in an enlarged decay region was then used to compute the momentum vector of the parent neutral particle. Event candidates were then formed by a vertex fit using all combinations of a neutral-particle trajectory and the remaining interaction vertex track candidates that satisfied the trigger topology; here the trigger required a V plus two additional charged tracks. In the case of multiple event interpretations, the interpretation with the lowest vertex χ^2 was chosen.

For physics analysis of reconstructed events, we demand that the interaction vertex be within

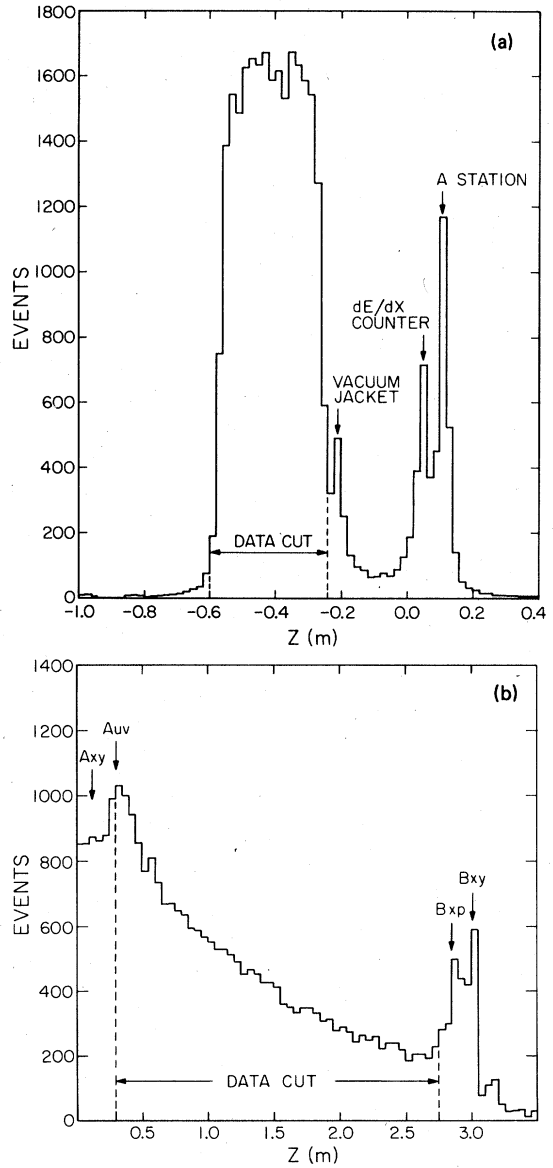

FIG. 3. (a) Interaction vertex distribution. (b) K^0 vertex distribution.

the hydrogen target as shown in Fig. 3(a). The z distribution of the secondary K^0 vertex [Fig. 3(b)] shows the expected exponential decay. A cut is made which requires that the K^0 decays between the A and B stations.

C. Čerenkov identification of the outgoing particles

The identification of the outgoing charged particles[6] was done by two large multicelled Čerenkov counters $\check{C}_1$ and $\check{C}_2$ (see Fig. 1). $\check{C}_1$ was filled with 100% air at atmospheric pressure with an index of refraction $n = 1.000\,29$ and had a radiator length of 4 m. Its active area was 4.5×1.5 m^2 with a mirror surface at about 12 m from the target. With 90% helium and 10% air, C_2 had an index $n = 1.000\,06$ and had a radiator length of 8.4 m. The active area of 4.0×2.1 m^2 was at a distance of about 23.6 m from the target center. The relative yield of Čerenkov light as a function of momentum is plotted in Fig. 4. The sampling of Čerenkov light was achieved in $\check{C}_1$ by 18 cells each with a foam-backed aluminized Mylar mirror, a Winston cone, and an RCA 4522 phototube. $\check{C}_2$ has 16 cells each with an aluminized $\frac{1}{4}$-in Lucite mirror, a Winston cone, and an RCA 8854 Quanticon phototube.

Mean photoelectron yields for each phototube were obtained by using data from the reaction $\pi^- p \to \pi^+ \pi^- n$ at 100 GeV/c. Momentum, pulse height, and geometrical cuts were made to ensure a reliable pion signal.

The particle identification was governed by the production or nonproduction of light (see Fig. 4). Identification criteria were combined into the analysis programs where the maximum-likelihood method was used. The assumption was made that the photoelectron number measured by the phototubes is Poisson distributed. Geometrical effects were taken into account (for example, a particle hitting an edge or a corner of a cell).

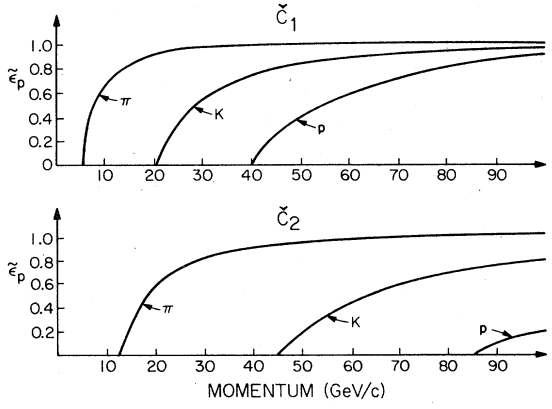

FIG. 4. Relative yield of Čerenkov light $[\tilde{\epsilon}_p = (1 - 1/n^2)^{-1}(1 - 1/n^2\beta^2)]$ as a function of momentum.

For each event we consider all possible types (π, K, or p) for the final particles (i.e., 3^4 hypotheses for a four-particle final state). For each hypothesis we calculate the likelihood of the observed photoelectron yield in the 34 cells.[8] More precisely, if there are k particles of masses $m_1, \ldots, m_k$, i.e., a combination of types $a_1, \ldots, a_k$, where $a_i = 1, 2, 3$, depending on whether the particle is hypothesized as a pion, kaon, or proton, then one can predict the number of photoelectrons seen by the jth phototube. This can be written as

$$n_j(c_i) = \sum_{l=1}^{k} \lambda_j(l, a_l^i), \tag{2.1}$$

where

$c_i = (a_1^i, \ldots, a_k^i) = i$th combination of particles for that event, $l = l$th track in an event, $l = 1, \ldots, k$.

The logarithm of the probability or likelihood of observing tracks $1, \ldots, k$ as the combination of particles $c_i = (a_1^i, \ldots, a_k^i)$ is

$$L(c_i) = \ln p(c_i) = \ln \prod_{j=1}^{34} \frac{[n_j(c_i)]^{n_0^j} e^{-n_j(c_i)}}{\Gamma(n_0^j + 1)}, \tag{2.2}$$

where $n_j(c_i)$ is defined above and where $n_0^j =$ observed number of photoelectrons in the jth cell. Note that the $\Gamma(n_0^j + 1)$ function is used instead of $n_0^j!$, since n_0^j as defined is not restricted to integer values.

If all of the information about the particle is combined into a single number or likelihood, the best fit to the types in a given event will simply give the largest likelihood. Above 45 GeV/c and below 6 GeV/c, the differentiating power of the Čerenkov counters is lost. The decays of $K^0 \to \pi^-\pi^+$ and $\phi \to K^+K^-$ serve as a test case for the particle-identification system and determine the pion and kaon detection efficiencies. The pion detection efficiency is 90% for a "tight cut" in the likelihood $[L(K^-\pi^+\pi^-) - L(K^-K^+\pi^-) \geq 10.0]$ and is 96% for a "loose cut" $[L(K^-\pi^+\pi^-) - L(K^-K^+\pi^-) > -2.0]$. For kaon detection efficiency, the "tight cut" $[L(K^\mp\pi^\pm K^0) - L(KKK^0) \leq -2.0]$ had an efficiency of 71%, while the "loose cut" $[L(K^\mp\pi^\pm K^0) - L(KKK) < 0]$ had a 93% efficiency.

III. $K^0K^\pm\pi^\mp$ FINAL STATES

The $K^0K^\pm\pi^\mp$ final states[9] will be discussed first. Tight Čerenkov cuts (see Sec. IIB) were imposed on the interaction-vertex particles, $L(\pi^-\pi^+K^0) - L(K^\pm\pi^\mp K^0) \geq 10.0$ for pions and $L(\pi^-\pi^+K^0) - L(K^\pm\pi^\mp K^0) \leq -2.0$ for kaons. Both particles from the interaction vertex are required to be in the 6–45 GeV/c band and a mass cut $(0.47 \leq m_{K^0} \leq 0.53$ GeV) is made on vee particles. Also, a

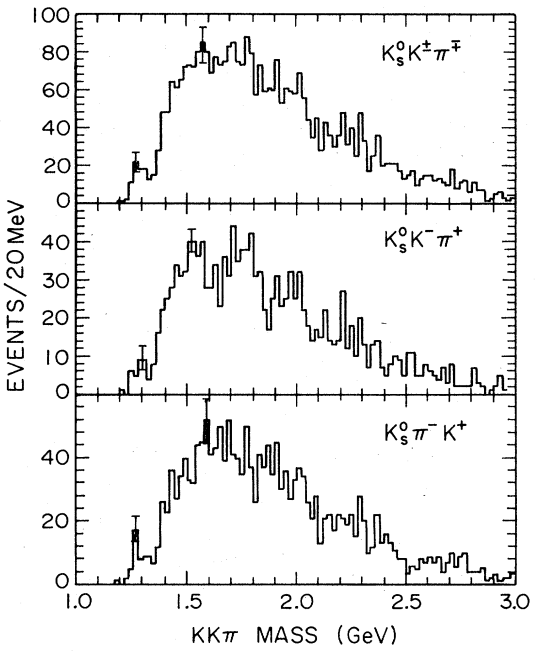

FIG. 5. $KK\pi$ mass distribution.

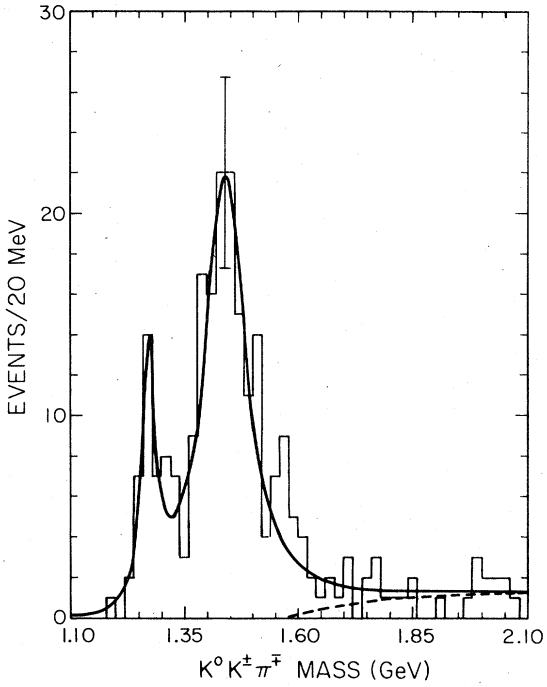

FIG. 6. $K^0K^{\pm}\pi^{\mp}$ mass distribution with δ cut [$M(K^0K^{\pm}) \leq 1.04$ GeV]. The full line refers to a resonance plus background fit and the dashed line is the background fit.

loose cut is made on the K^0, that is, both the likelihood difference between $K\pi K^0$ and $K\pi\overline{\Lambda}$ and the likelihood difference between $K\pi K^0$ and $K\pi\Lambda$ are greater than -2.0. This guarantees a high efficiency and yet a relatively pure sample of K^0. The mass spectra of the $K^0K^{\pm}\pi^{\mp}$, $K^0K^-\pi^+$ and $K^0\pi^-K^+$ systems are shown in Fig. 5. No obvious resonance signals are observed in these spectra.

The $K^0K^{\pm}\pi^{\mp}$ mass spectrum requiring a "δ cut" [$M(K^0K^{\pm}) \leq 1.04$ GeV] is shown in Fig. 6. A $D(1285)$ and $E(1420)$ are seen over little background. The contributions from the two charged modes are equal as expected; the two modes have been combined to increase the statistics. Two types of fits are done (see Table I for results). The first is a fit to two Breit-Wigner resonances plus a background, which underestimates the background near the E region. To obtain a better estimate of the background, a sample of $\pi^+\pi^-K^0$ events was deliberately misidentified as being $K^{\pm}\pi^{\mp}K^0$ and the δ cut was made. This "background", which was smoothly varying and had no enhancements, was then subtracted from the true $K^{\pm}\pi^{\mp}K^0$ events and a fit was made to two Breit-Wigner resonances (see Fig. 7). The results, compared with the world average[1] and recent results,[2-4] are shown in Fig. 8. The various resolu-

TABLE I. E production in $\pi^-p \to K^0K^{\pm}\pi^{\mp}\tilde{X}$.

	$\sigma\pi$ mode	$K^{*0}K^0$ and $K^{*\pm}K^{\mp}$ modes	$K^{*\pm}K^{\mp}$ mode	$K^{*0}K^0$ mode
Resonance-plus-background fit				
Mass (MeV)	1440 ± 6	1458 ± 7	1447 ± 6	1454 ± 15
Width (MeV)	110 ± 27	71 ± 31	71 ± 15	71 ± 75
Background-subtracted fit				
Mass (MeV)	1440 ± 5	1460 ± 20	1433 ± 14	1433 ± 25
Width (MeV)	62 ± 14	47 ± 58	71 ± 33	71 ± 62

δ cut: $M(K^0K^{\pm}) \leq 1.04$ GeV
K^* cut: $0.84 \leq M(K\pi) \leq 0.94$ GeV

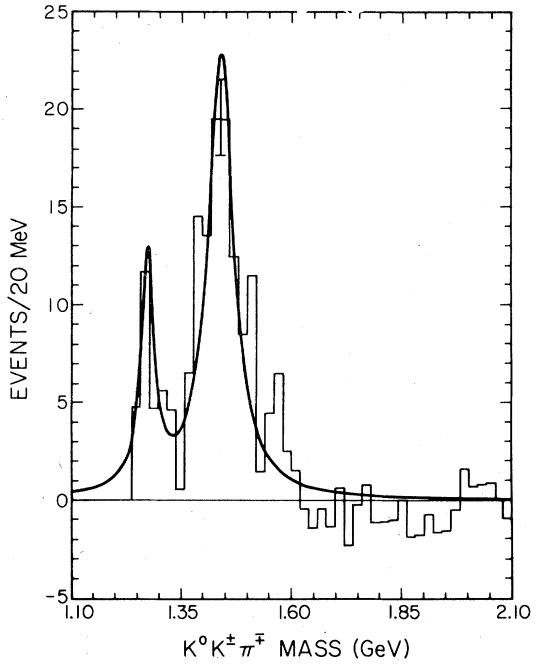

FIG. 7. $K^0K^\pm\pi^\mp$ mass distribution with δ cut [$M(K^0K^\pm) \leq 1.04$ GeV] and background subtracted. The full line refers to a resonance fit.

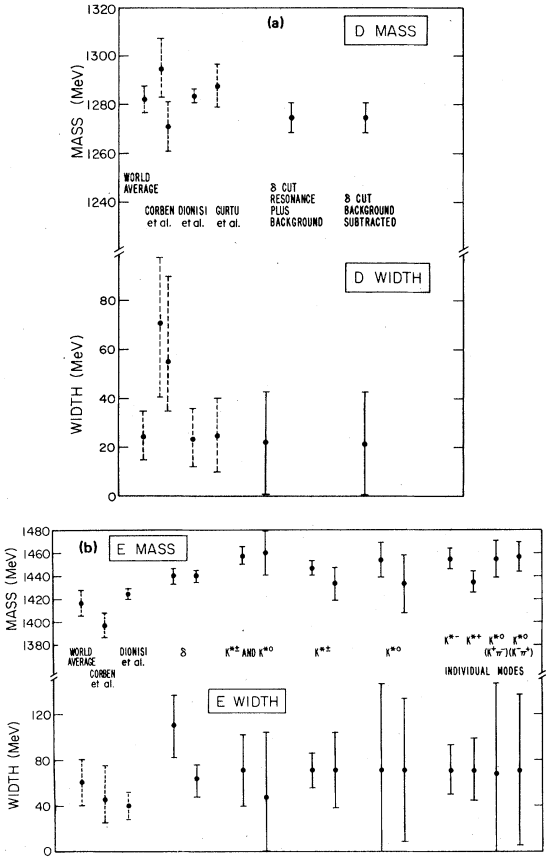

FIG. 8. (a) Comparison of D mass and width results. Corden *et al.* report two values; the first is the result for the $\eta^0\pi^+\pi^-$ decay mode and the second is for the $K^+K^-\pi^0$ decay mode. (b) Comparison of E mass and width results. If two values are presented, the first is the result of a resonance-plus-background fit and the second is the background-subtracted-fit result.

tions have been calculated using the error matrix from the fitting program. The mean mass resolution of the $\delta\pi$ state is 30.4 ± 0.8 MeV at 100 GeV/c and 16.4 ± 0.9 MeV at 50 GeV/c. The results of fits presented here have included the unfolding of the resolution. The agreement of the D mass and width with other results is very good. The width of the E obtained with the background-subtracted fit agrees well with the others, while the E mass is slightly high (less than one standard deviation, however).

The D cuts [$1.257 \leq m(KK\pi) \leq 1.307$ GeV] were imposed on the $K^0K^\pm\pi^\mp$ mass spectrum with the resulting two-body mass spectra shown in Fig. 9. A "δ enhancement" is seen in $K^0K^\mp$ peaking near the threshold. The corresponding E cut [$1.356 \leq m(KK\pi) \leq 1.476$ GeV] spectra are shown in Fig. 10. An enhancement is present both in the $K^\pm\pi^\mp$ and $K^0K^\pm$ indicating $K^*(890)$ and δ production.

K^* cuts [$0.84 \leq m(K\pi) \leq 0.94$ GeV] were applied and the resulting $K^0K^\pm\pi^\mp$ mass spectra are shown in Fig. 11. An E signal is seen (note that the D-meson region is below K^*K threshold). The largest signal-over-background ratio is obtained when we demand that both $(K\pi)^0$ and $(K\pi)^\pm$ be in the K^* region [see Fig. 11(a)]. This cut reduces the amount of background present. The signal-to-background ratio is larger when one requires the charged $K\pi$ combination rather than the neutral combination to be in the K^* region [see Figs. 11(b), 11(c), and Table I]. Again a sample of $K\pi\pi$ events was deliberately misidentified as $KK\pi$ and a K^* cut was imposed. This background was subtracted from the true events and the difference was fitted to a Breit-Wigner resonance. Both the results from the resonance-plus-background fit and the background-subtracted fit are shown in Table I. The mean resolution of the K^*K mass is 36.9 ± 0.6 MeV at 100 GeV and 19.4 ± 0.8 MeV at 50 GeV. The fits have included the unfolding of the resolutions. A resonance-plus-background fit (statistics were too low for a background subtracted fit) was performed on the individual modes (Table II). With the limited statistics, the number of events from each model is equal as expected. While the E meson signal is seen with a K^* cut, it has a better signal-to-background ratio with a "δ cut." Therefore, the background-subtracted fit

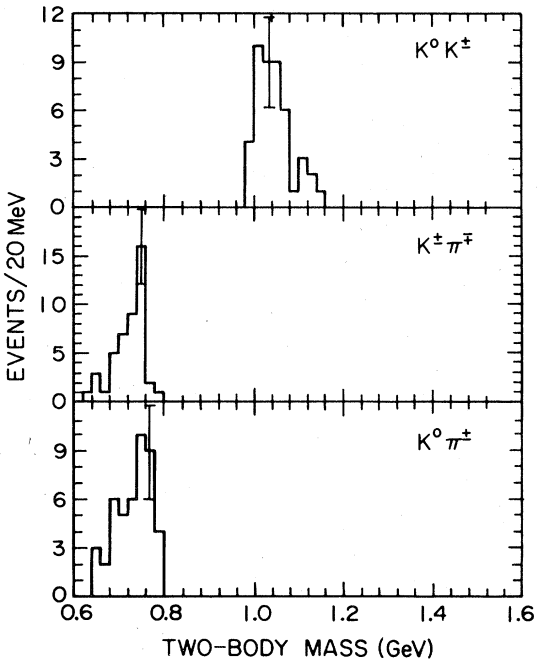

FIG. 9. Two-body mass distribution with D cut [1.257 $\leq M(KK\pi) \leq$ 1.307 GeV].

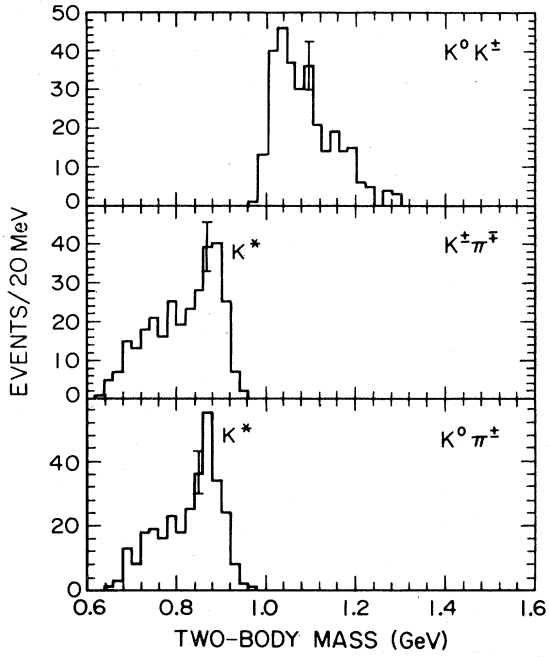

FIG. 10. Two-body mass distribution with E cut [1.356 $\leq M(KK\pi) \leq$ 1.476 GeV].

with a δ cut is presented as the best fit. Dionisi *et al.*[3] obtained as a result of a partial-wave analysis a branching ratio $E \to K^*\bar{K} + \bar{K}^*K/E \to [\delta\pi + (K^*\bar{K} + \bar{K}^*K)] = 0.86 \pm 0.12$, where $\delta \to K\bar{K}$. Taking the ratios of cross section times branching ratio from Table V, we determined this branching ratio to be 0.76 ± 0.06, which is in agreement with their determination.

IV. $K^0K^+K^-$ FINAL STATE

The $K^0K^+K^-$ final state[10] has been studied for resonance structure from the reaction $\pi^-p \to K^0K^+K^-\bar{X}$. The data sample is small (only 9% of the vee-plus-two-charged-particle events); therefore, we have maximized the event number by using the loose Čerenkov cut on the interaction-vertex particles [see Sec. IIC; $L(\pi^-\pi^+K^0) - L(K^-\pi^+K^0) < 0$ and $L(\pi^-\pi^+K^0) - L(\pi^-K^+K^0) < 0$ or equivalently $L(\pi^-\pi^+K^0) - L(K^-K^+K^0) < 0$]. Both interaction-vertex particles are required to be in the 6–45 GeV/c band and a mass cut ($0.47 \leq m \leq 0.53$ GeV) is made on vee particles. Also, the loose Čerenkov cut is made on the K^0. Both the likelihood difference between $K^-K^+K^0$ and $K^-K^+\Lambda^-$ and the likelihood difference between $K^-K^+K^0$ and $K^-K^+\Lambda$ are greater than -2.0. These requirements provide a high number and retain a relatively pure sample of K^0. The $K^0K^-K^+$ mass spectrum is shown in Fig. 12.

$K^0\phi$ final state

A well-defined ϕ signal is observed in the K^+K^- mass spectrum (see Fig. 13). A ϕ cut ($1.01 \leq M(K^+K^-) \leq 1.03$ GeV) is imposed and the resultant $K^0K^+K^-$ mass spectrum is shown in Fig. 14. A low-statistics enhancement is seen in the 1.82–1.86 GeV bin. Examining the spectra in finer bins (20 MeV), the events are centered toward the higher half of the bin. The ϕ's in our data are produced preferentially at high total momentum [or high x, where $x = P_{\text{tot}}{}^{(K^0K^-K^+)}/P_{\text{incident}}$]. For $x \geq 0.9$, the ϕ cut [$1.01 \leq M(K^+K^-) \leq 1.03$ GeV] produces a data sample which is almost pure resonance (82%), while for $x < 0.9$, the cut produces a less pure (65%) signal. Therefore, making a ϕ cut along with an x cut ($x \geq 0.9$) should greatly increase the resonance to background ratio. The resultant $K^0K^-K^+$ spectra (Fig. 15) show the corresponding increase in the resonance-signal-to-background ratio. The 20-MeV binning again shows that more events are centered toward the higher half of the bin. A fit to a resonance plus background gives a mass of 1842 ± 9 MeV and a width of 35 ± 30 MeV. Since the number of events is small, Poisson statistics should be applied. A relevant measure of the significance of these results is the probability of such an event occurring. The probability of obtaining a signal of 10 when one expects a signal of 1.4 (the background—see

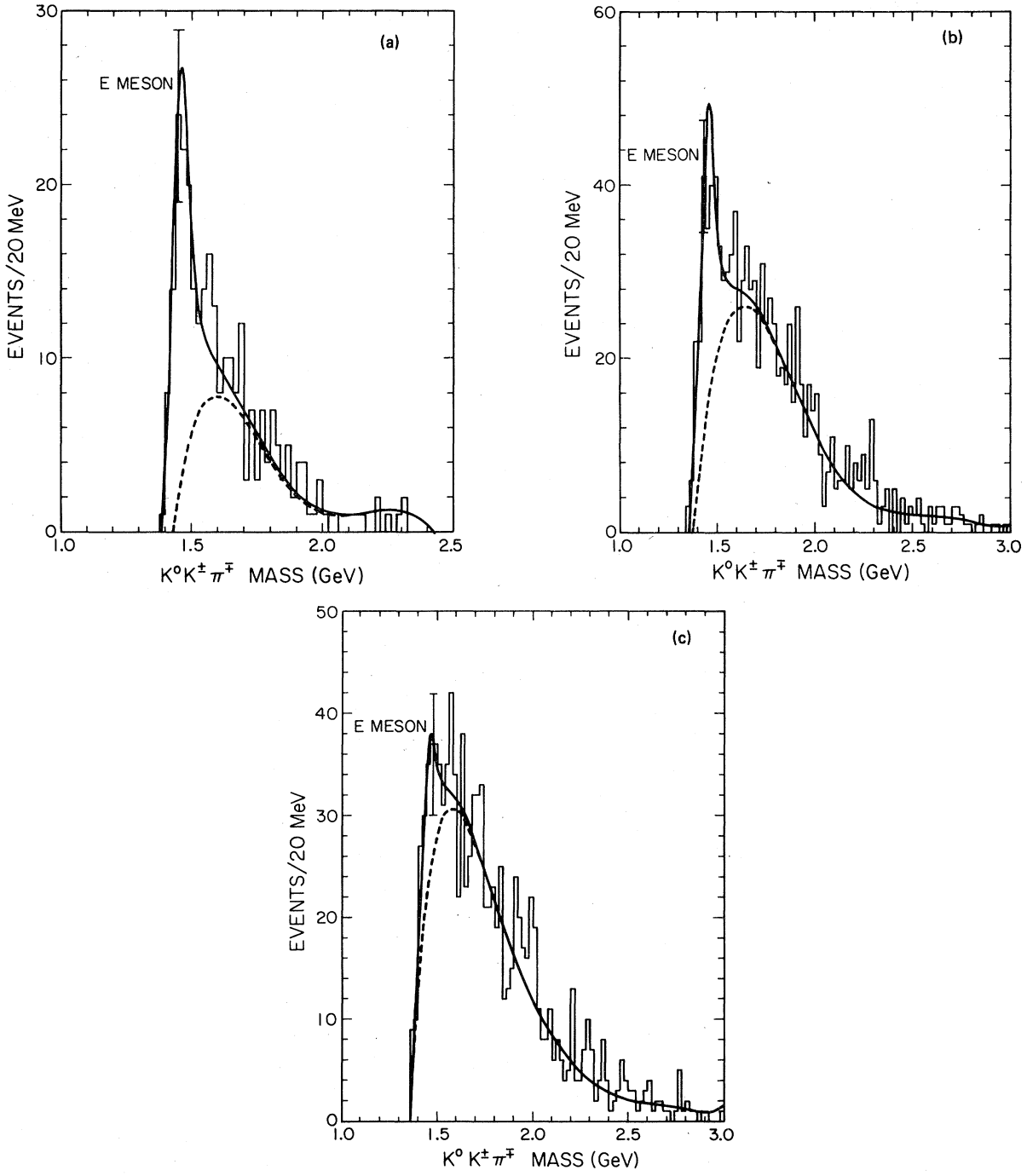

FIG. 11. (a) $K^0K^\pm\pi^\mp$ mass distribution with K^{*0} and K^{**}cut [$0.84 \leq M(K\pi) \leq 0.94$ GeV]. (b) $K^0K^\pm\pi^\mp$ mass distribution with $K^{*\pm}$ cut [$0.84 \leq M(K\pi)^\pm \leq 0.94$ GeV]. (c) $K^0K^\pm\pi^\mp$ mass distribution with K^{*0} cut [$0.84 \leq M(K\pi)^0 \leq 0.94$ GeV].

Fig. 15) is 2×10^{-6}. As a check, the $K\pi\pi$ and $KK\pi$ systems have been deliberately misidentified as the $3K$ system and the "ϕ" cut has been made. No peak occurred in either the $KK\pi$ or the $K\pi\pi$ system. As a further check, tighter Čerenkov cuts were imposed on the interaction vertex particles [$L(\pi^-\pi^+K^0) - L(\pi^-K^+K^0) \leq -2$ and $L(\pi^-\pi^+K^0) - L(K^-\pi^+K^0) \leq -2$ or equivalently $L(\pi^-\pi^+K^0) - L(K^-K^+K^0) \leq -3$] The $3K$ enhancement remained. A cut was made on the $3K$ mass [$1.82 \leq M(3K) \leq 1.86$ GeV) with the corresponding two-particle mass plots given in Fig. 16. A large ϕ production

TABLE II. E production by individual modes in $\pi^- p \to K^0 K^\pm \pi^\mp \tilde{X}$.

	$K^{*-}K^+$ mode	$K^{*+}K^-$	$K^{*0}(K^+\pi^-)K^0$ mode	$K^{*0}(K^-\pi^+)K^0$ mode
Mass (MeV)	1455 ± 9	1435 ± 9	1455 ± 16	1457 ± 13
Width (MeV)	71 ± 22	71 ± 27	68 ± 79	71 ± 66
Number of events in peak	99 ± 22	90 ± 23	59 ± 73	70 ± 72

δ cut: $M(K^0K^\pm) \leq 1.04$ GeV
K^* cut: $0.84 \leq M(K\pi) \leq 0.94$ GeV

is seen in the K^+K^- spectrum. Therefore, we conclude that this $3K$ enhancement has the following decay mode: $K^* \to K^0\phi$, $\phi \to K^+K^-$.

The widths of the K^* and ϕ resonances are rather narrow and are consistent with the resolution of the spectrometer for these final states. The various resolutions are calculated using the error matrix from the fitting program. The mass resolution in the ϕ mass region is small (the mean resolution $\delta M_{\text{mean}} = 0.8 \pm 0.2$ MeV at 50 GeV/c and 1.7 ± 0.2 MeV at 100 GeV/c), and thus the natural decay width dominates in the plot of Fig. 13. The ϕ's are well resolved since their decay products (the K^+ and K^-) have low ϕ center of mass momenta (low Q value for the ϕ decay) and all chambers may be utilized in fitting these tracks. The largest uncertainty comes from the K^0 resolution ($\delta M_{\text{mean}} = 14.6 \pm 0.9$ MeV and 22.6 ± 0.7 MeV at 100 GeV/c). Here one must not only fit the tracks with fewer chambers (remember the K^0 must decay between the A and B chambers) but also do a vertex determination. The final calculated mean resolution of the $K^0\phi$ state is 21 ± 2 MeV at 50 GeV/c and 35 ± 2 MeV at 100 GeV/c. Since the majority (93%) of data is from 100 GeV/c, the resolution of 35 ± 2 MeV will dominate. Therefore, the width of the resonance is consistent with the resolution of the experiment. The charmed D^0 meson, a narrow state, has a mass of 1863.28 ± 0.86 MeV.[1] Taking account of our limited statistics and systematic measurement errors, we feel that the enhancement is consistent with being the charmed D^0.

Such a decay of the charmed D^0 would be explained by the diagram of Fig. 17(a) and its conjugate. Here the D^0 ($c\bar{u}$) decays by the exchange of a W and an $\bar{s}s$ pair is created. Similarly, one would expect decays with a creation of $\bar{d}d$ and $\bar{u}u$ pair [Figs. 17(b) and 17(c)] with a comparable probability. [Maybe the light quark processes are about twice the size of the contribution of Fig. 17(a), where the $s\bar{s}$ is created from the vacuum.] Be-

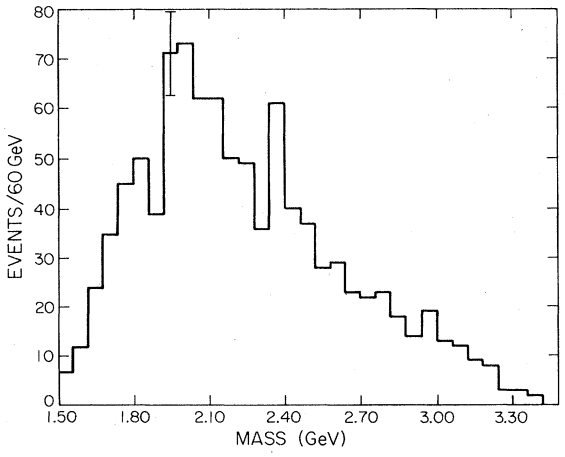

FIG. 12. $K^0K^+K^-$ mass spectrum.

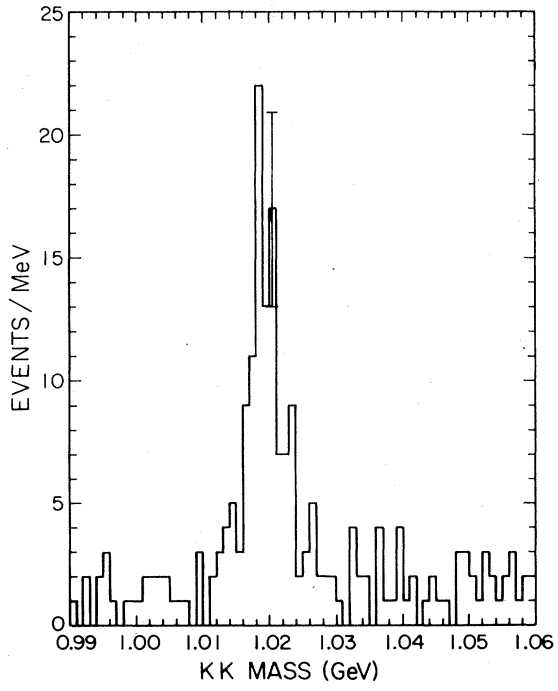

FIG. 13. K^+K^- mass distribution.

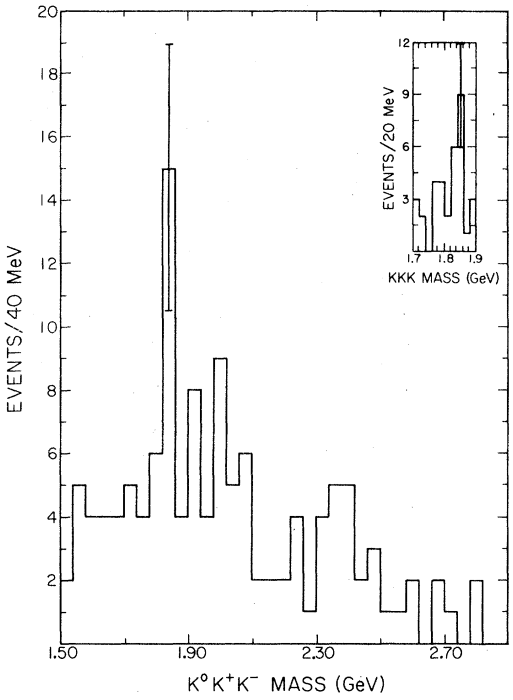

FIG. 14. $K^0K^+K^-$ mass distribution with ϕ cut [1.01 $\leq M(K^+K^-) \leq$ 1.03 GeV].

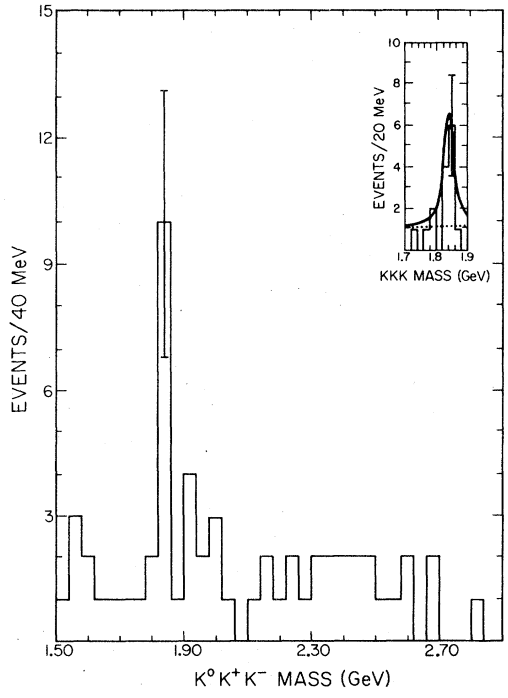

FIG. 15. $K^0K^+K^-$ mass distribution with ϕ [1.01 $\leq M(K^+K^-) \leq$ 1.03 GeV] and x ($x \geq 0.90$) cuts.

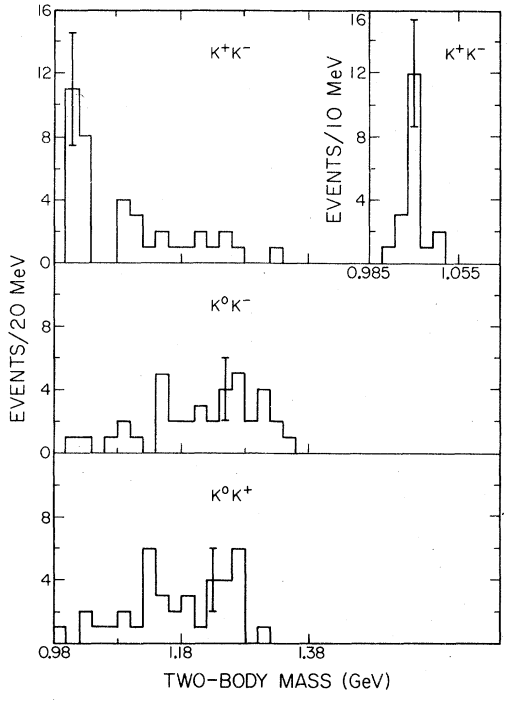

FIG. 16. Two-body mass distribution with the cut [1.82 $\leq M(K^0K^+K^-) \leq$ 1.86 GeV].

cause the vee-plus-two-charged-particles trigger discussed here also includes the state $K^0\pi^+\pi^-$, the diagram of Fig. 17(c) and its conjugate can be studied. The $K^{**}\pi^{\mp}$ mode is investigated, since the decay of the D via $K^*(890)$ has been reported in pp collisions.[11] The $K^0\pi^+$ [Fig. 18(a)] spectrum has a large K^{*+} signal, while the $K^0\pi^-$ [Fig. 18(b)]

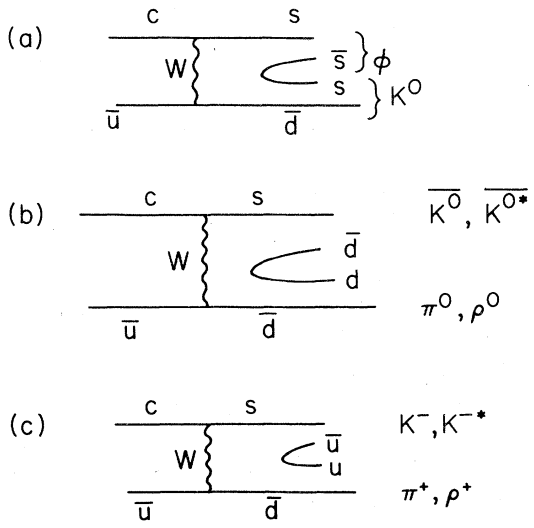

FIG. 17. Diagrams for charmed D^0 decay.

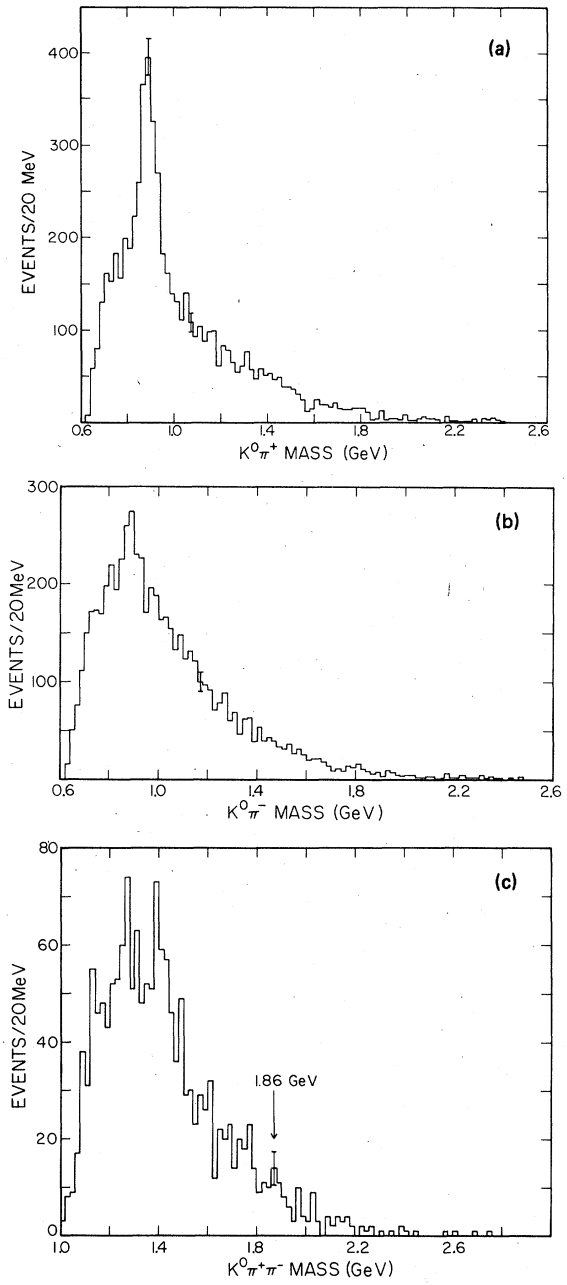

FIG. 18. (a) $K^0\pi^+$ mass spectrum from the $K^0\pi^+\pi^-$ data. (b) $K^0\pi^-$ mass spectrum from the $K^0\pi^+\pi^-$ data. (c) $K^0\pi^+\pi^-$ mass spectrum with K^{*+} cut [$0.84 \leq M(K^0\pi^+) < 0.94$ GeV].

distribution has a weaker K^* signal. Making a K^{*+} cut [$0.84 \leq M(K^0\pi^+) < 0.94$ GeV], the $K^0\pi^+\pi^-$ mass spectrum is shown in Fig. 18(c). Since we are selecting the K^{+*} mode (no K^{-*}) and the $K^0\pi^+$ decay is observed only (no $K^+\pi^0$), the ratio of the observed decay of diagram Fig. 17(a) to 17(c) would be reduced from about 1:2 to 1:$\frac{2}{3}$. Our $K^0\phi$ resonance signal at the D^0 mass is 10 events

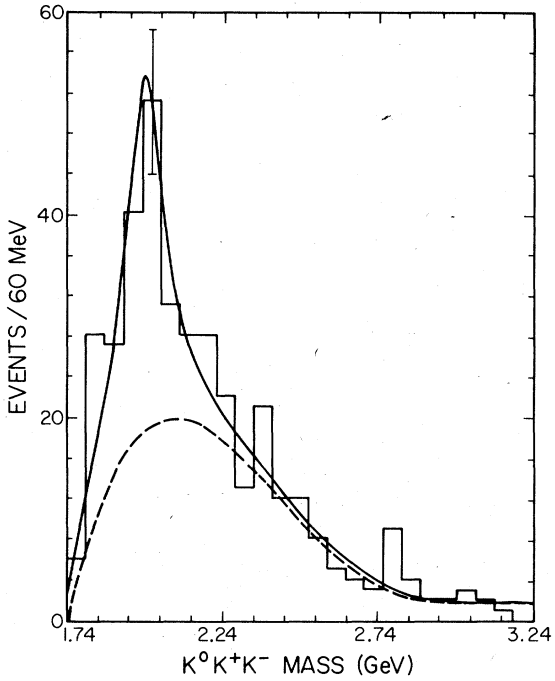

FIG. 19. $K^0K^+K^-$ mass distribution with A_2 cut [$1.261 \leq M(KK) \leq 1.363$ GeV].

(100 and 50 GeV/c data combined) with a background of 5. Hence we would expect a signal of about 8 from the $K^{*+}\pi$ mode. Examining Fig. 18(c), we find the data are consistent with this expectation but there is no statistically significant effect.

Charmed baryons and mesons have been observed in hadronic experiments and their results are summarized in Table IV. The cross sections times branching ratios serve as a check. Since the results here are semi-inclusive and serve as a lower limit for a truly inclusive reaction, one would expect this cross section times branching ratio to be much smaller than the other results. This is indeed the situation.

KA_2 final state

The mass spectrum requiring $M(K^+K^-)$, $M(K^+K^0)$, or $M(K^-K^0)$ to lie in the A_2 mass region (1.261 to 1.363 GeV) is shown in Fig. 19. A rather striking peak is seen at 2.0 GeV. Examining the different modes A_2^0, A_2^-, and A_2^+, the contribution from each is approximately equal as expected (Fig. 20 and Table III). A clear peak is seen with the A_2^0 cut, while a shoulder on the peak exists for the $A_2^\pm$ modes. This is explained by kinematic reflection. When one does an $A_2^\pm$ cut (in this case with [$1.80 \leq M(3K) \leq 2.10$ GeV]), some ϕ contribution is also obtained. This shoulder is associated with the $K\phi$ enhancement. If one subtracts the A_2^0 signal from both the $A_2^\pm$ contributions, a signal (with poor sta-

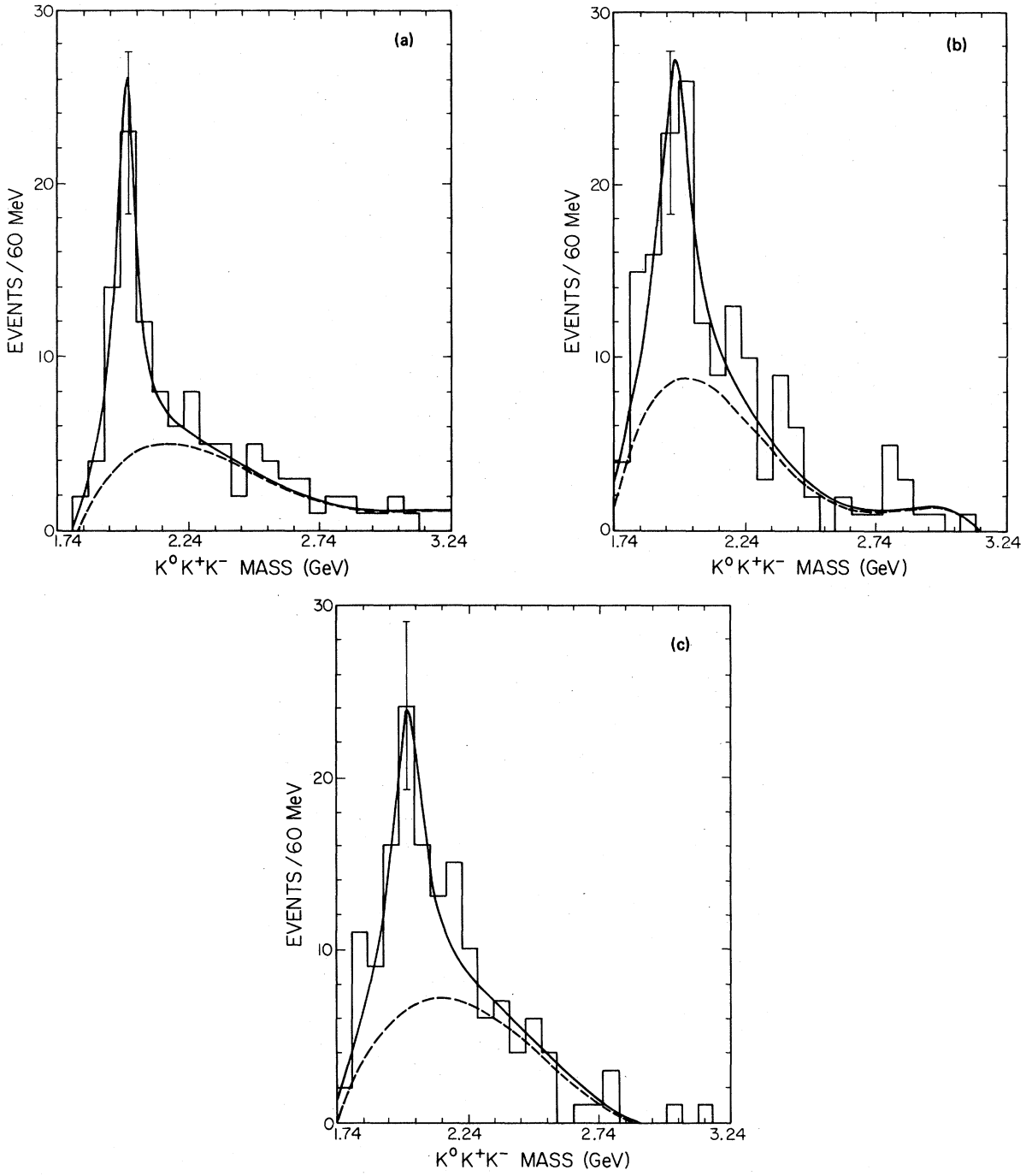

FIG. 20. (a) $K^0K^+K^-$ mass distribution with A_2^0 cut [$1.261 \leq M(K^+K^-) \leq 1.363$ GeV]. (b) $K^0K^+K^-$ mass distribution with A_2^- cut [$1.261 \leq M(K^0K^-) \leq 1.363$ GeV]. (c) $K^0K^+K^-$ mass distribution with A_2^+ cut [$1.261 \leq M(K^0K^+) \leq 1.363$ GeV].

tistics) is seen near 1.8 GeV. Since the A_2^0-cut signal is the cleanest (being unaffected by this kinematic reflection), its fit is taken as the best value. The resonance plus background fit gives a mass of 2003 ± 14 MeV with a width of 87 ± 43 MeV. A cut [$1.92 \leq M(3K) < 2.10$ GeV] is imposed with the resulting two-body spectra given in Fig. 21.

As a check, the $K\pi\pi$ and $KK\pi$ events were deliberately misidentified as KKK, and the A_2 cuts were imposed. The resulting three-body spectrum shows no signs of the enhancement and looks very much like a background. Further, tight

TABLE III. K^* (2000) production. Results of resonance plus background fits with both 50 and 100-GeV/c data.

Cut	A_2^{all}	$A_2^0 \to K^+K^-$	$A_2^- \to K^0K^-$	$A_2^+ \to K^0K^+$
Mass (MeV)	1986±15	2003±14	1968±20	2009±20
Width (MeV)	150±68	87±43	136±90	150±78
Number of events	137±60	50±20	66±44	68±31

Čerenkov cuts (see ϕ section) were used and this enhancement is still clearly present.

The mass resolution was calculated from the fitting program error matrix for the KA_2 final state (at 50 GeV/c, $\delta M_{mean} = 17.8 \pm 0.7$ MeV at 100 GeV/c, $\delta M_{mean} = 32.7 \pm 0.8$ MeV). The width of this state (87±43 MeV) is wider than the resolution and hence it is inconsistent with a very narrow state. The excited charmed D^{0*}, where the mass is consistent with this value, would not be expected to have a KA_2 mode, as it decays into $D^0\pi^0$ or $D^0\gamma^0$. This enhancement associated with KA_2 would therefore be an "ordinary" K^* resonance.

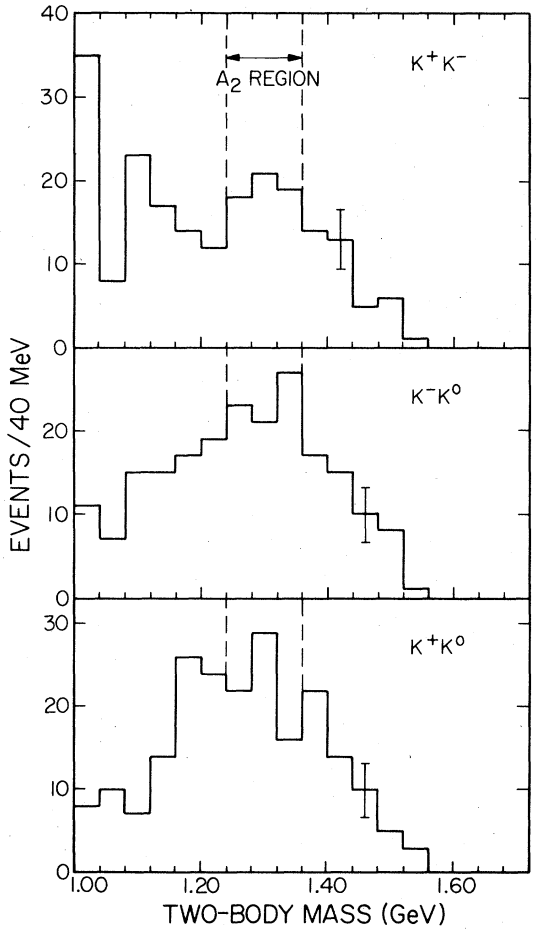

FIG. 21. Two-body mass distribution with the cut $[1.92 \leq M(3K) < 2.10$ GeV].

Other cuts

The following cuts produced no significant structure in the $K^0K^+K^-$ spectrum:

(a) δ $[M(K^\pm K^0) \leq 1.10$ GeV, $1.04 < M(K^+K^-) \leq 1.10$ GeV],

(b) f $[1.48 \leq M(K^+K^-) \leq 1.55$ GeV],

(c) g $[1.60 \leq M(K^+K^-, K^0K^\pm) \leq 1.78$ GeV],

(d) h $[1.94 \leq M(K^+K^-) \leq 2.14$ GeV].

V. CROSS SECTIONS TIMES BRANCHING RATIOS AT 100 GeV

The one-vee, two-prong semi-inclusive trigger is used to study the reactions $\pi^-p \to K^0K^\pm\pi^\mp\tilde{X}$ and $\pi^-p \to K^0K^+K^-\tilde{X}$, where $\tilde{X}$ is not completely inclusive. We require a specific forward topology of charged particles and an interaction registering in the cylindrical counters surrounding the target. Thus, events with extra forward charged particles or only recoil neutrons are suppressed, while neutral particles such as K^0 and π^0 $(\to \gamma\gamma)$ are allowed in all directions. Any number of slow charged particles (fragments of the target) are allowed. These cross sections should be viewed as lower bounds for a true inclusive production cross sections times branching ratios. Estimates of systematic and statistical errors are given separately.

As an example of the forward charged particle bias, an event would be vetoed by the first proportional counter (A station) if it had an extra $\pi^\pm$ of $p_\perp \approx 300$ MeV with only about 1.3 GeV or more of forward momentum. Events of the type $\pi^-p \to K^0K^-\pi^+n$ would only trigger about 10% of the time.

The data described here have an average forward total momentum (of the measured charged particles) of 70 to 80 GeV depending on the reaction. A typical event has about 25 GeV on missing energy (fast forward neutrals and wide-angle charged and neutral debris, $\tilde{X}$). The entire momentum range has been used as input in the analysis. After various cuts including Cerenkov cuts, the momentum distribution ranges from approximately 30 to 100 GeV.

The cross sections times branching ratios were found in a two-step procedure. The D and E deter-

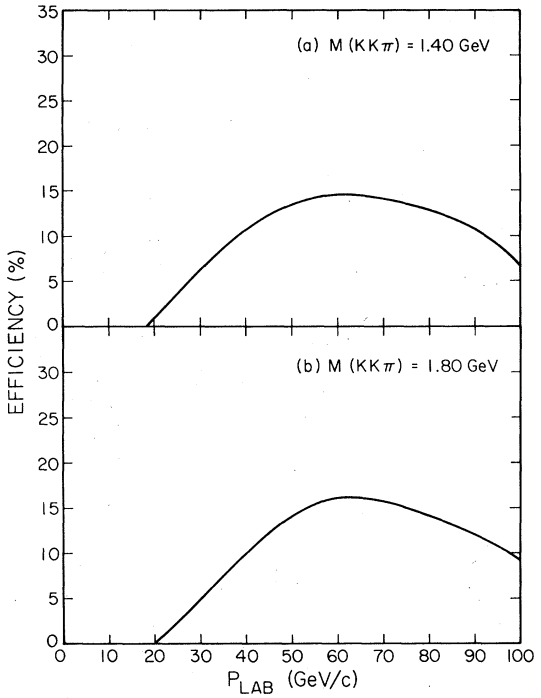

FIG. 22. Monte Carlo results for $KK\pi$ using δ decay mode.

minations are used as an example.

First, the cross section (without acceptance and other loss corrections) for $\pi^- p \to K^0 K^\pm \pi^\mp \bar{X}$ is found. This value applies to the entire $K^0 K^\pm \pi^\mp$ mass spectrum before any of the two-body mass cuts are applied. Next, the fraction of $K^0 K^\pm \pi^\mp$ events in the resonant signals is found and corrections are made for acceptance and other losses. All mass spectra presented in this paper are uncorrected for acceptance and trigger efficiency.

The acceptance for events of our trigger topology was calculated using a Monte Carlo program which modeled the multiparticle spectrometer. The program-generated events with the vertex randomized within the hydrogen target and with a transverse momentum (300 MeV/c) given by $d\sigma/dt \propto e^{-6p_\perp}$. The identification efficiencies (see Sec. II C) of the Čerenkov counters C_1 and C_2 are taken into account and thus the momenta of the two main vertex particles are required to be in the 6–45 GeV/c band. The trigger requirements (see Sec. II A) involving A, B, C, and D counters were imposed. The size, position, and efficiencies of the counters required by the trigger were included. The finite granularity of the counters and the separation between the tracks were considered. The decay is assumed to proceed via two steps. For $KK\pi$, the modes of $\pi\delta$ and $K^0 K^*$ were used (see Figs. 22 and 23). For KKK, the decay was modeled to proceed either as $K^0\phi$ (Fig. 24) or as KA_2 (Fig. 25). The acceptance was found as a function of the three-particle mass and total momentum for the various decay cuts. No attempt has been made to consider losses which a truly inclusive trigger would introduce.

Average acceptance weights for the various

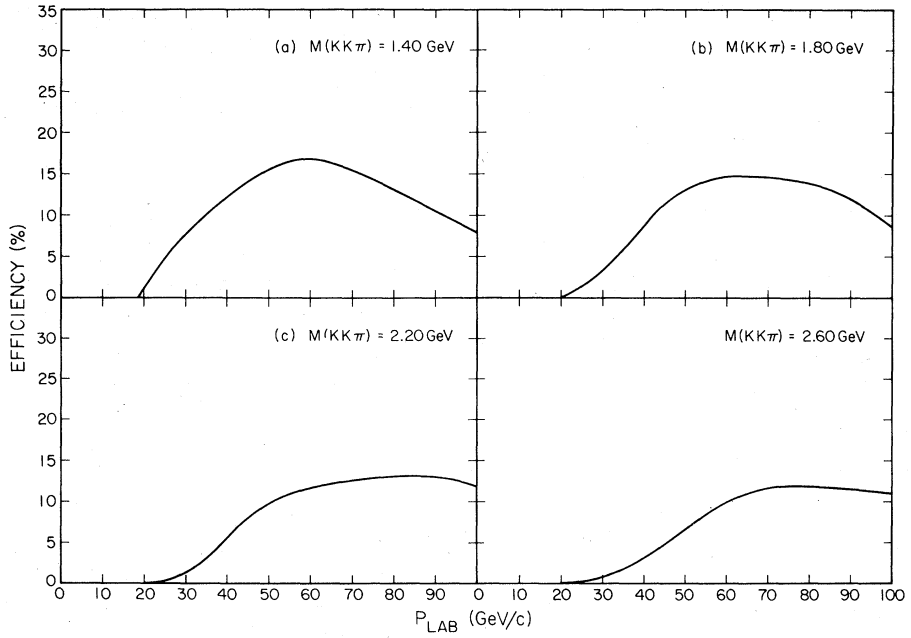

FIG. 23. Monte Carlo results for $KK\pi$ using K^* decay mode.

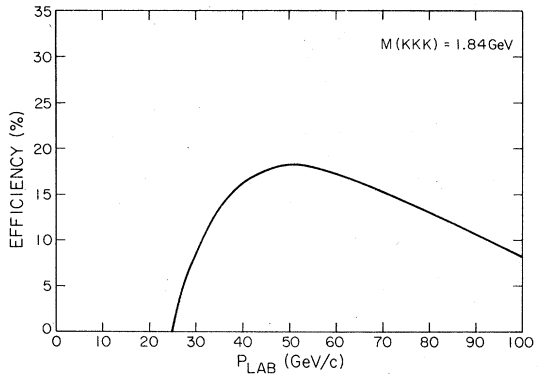

FIG. 24. Monte Carlo results for KKK using ϕ decay mode.

modes are listed below. A 20% systematic error is assigned to the weight:

$D(1285)$, δ cut, $\langle$ weight$\rangle = 12.9$
$E(1420)$, δ cut, $\langle$ weight$\rangle = 9.22$
$E(1420)$, K^{*0} cut, $\langle$ weight$\rangle = 8.46$
$E(1420)$, $K^{*\pm}$ cut, $\langle$ weight$\rangle = 8.53$
$K^0K^+K^-(1840)$, $\langle$ weight$\rangle = 10.3$
$K^0K^+K^-(2003)$, $\langle$ weight$\rangle = 4.73$.

Other corrections included are listed below:

$K_S^0 \to \pi^+\pi^-$ branching ratio, 68.61%.
Loss of events with K_L^0 instead of K_S^0, 50%.
Reconstruction efficiency (90 ± 10)%.
Losses from beam attentuation and secondary interactions in spectrometer material (12 ± 3)%.
Beam π fraction $e\mu$-contamination corrected (90 ± 3)%. [The beam Čerenkov program gives (93 ± 0.6)% for $\pi^-e^-\mu^-$ and special curve-through runs find 3.2% $e\mu$ contamination.]

Since the beam-π tagging efficiency was quite good (> 99.9%), no correction was applied. The track-finding efficiency was estimated to be 90 ± 10%.

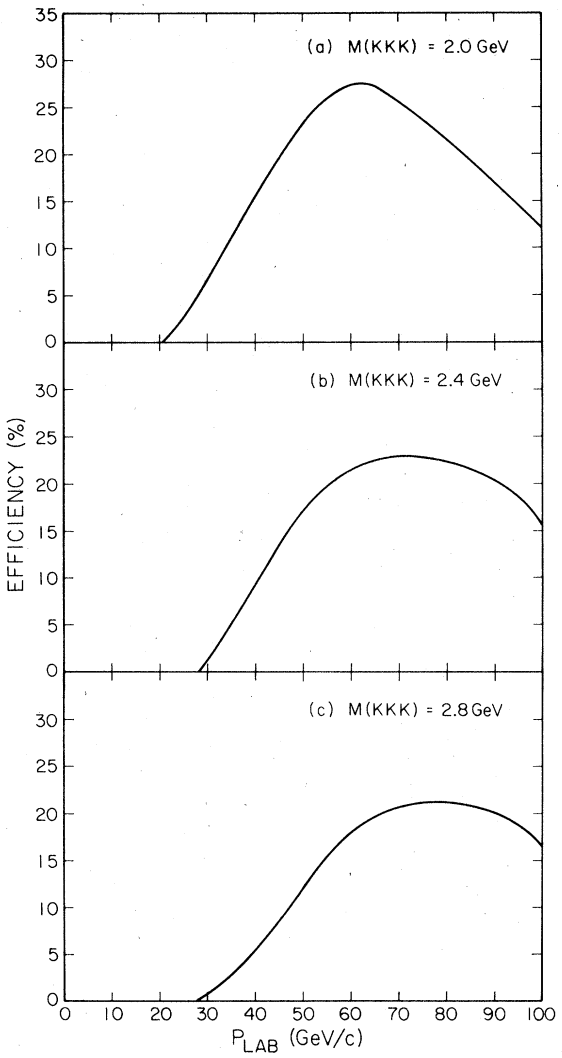

FIG. 25. Monte Carlo results for KKK using A_2 decay mode.

TABLE IV. Charmed-hadronic-production results.

Group	Mode	$\sigma \times B$ (μb)
This experiment	$D^0 \to \phi K^0 \to K^+K^-K^0$	0.5 ± 0.02[a]
D. Drijard *et al.* (Ref. 11)	$D^+ \to \bar{K}^{*0}\pi^+ \to K^-\pi^+\pi^+$	Range 4.0 to 62.0[b]
D. Drijard *et al.* (Ref. 12)	$\Lambda_c^+ \to \bar{K}^{*0}p$	6.2[b]
		3.0[b]
	$\Lambda_c^+ \to K^-\Delta^{++}$	6.7[b]
		3.3[b]
UCLA-Saclay (Ref. 13)	$\Lambda_c^+ \to \Lambda^0\pi^+\pi^+\pi^-$	2.8 ± 1.0
	$\Lambda_c^+ \to K^-\pi^+p$	2.3 ± 0.3
Giboni *et al.* (Ref. 14)	$\Lambda_c^+ \to \Lambda^0\pi^+\pi^+\pi^-$	$0.3 - 0.7$
	$\Lambda_c^+ \to K^-\pi^+p$	$0.7 - 1.8$

[a] Semi-inclusive result (lower bound for inclusive result).
[b] Results here are model dependent.

A detailed study has not been done, but a more refined value is not necessary for this analysis. The error in the beam π fraction was increased to include K^-, $\bar{p}$ contamination (<1%) effects. Overall, we estimate a systematic error of 25% in all the cross-section values listed. The cross sections are listed in Table IV. The only branching ratio corrected for was $K_S^0 \to \pi^+\pi^-/K_S^0 \to$ all.

The cross section times branching ratio for the $K^0\phi$ state is consistent with charmed D^0 production (see Sec. IV). Other hadronic charmed productions (see Table IV) have much larger cross sections than the one reported here. This is expected since our semi-inclusive value is viewed as a lower bound for a truly inclusive production result.

TABLE V. Cross section times branching ratio in μb at 100 GeV/c. Statistical errors only are included here. The uncorrected event count appears below each reaction. Reactions 1 and 2 use background-subtracted fits, while 3, 4, 5, and 6 use resonance-plus-background results.

Reaction	
1. $\pi^-p \to D(1285)\tilde{X}$ $\delta^\pm\pi^\pm \to K^0K^\pm\pi^\mp$ (31 ± 6)	0.18 ± 0.04
2. $\pi^-p \to E(1420)\tilde{X}$ $\delta^\pm\pi^\mp \to K^0K^\pm\pi^\mp$ (100 ± 10)	0.42 ± 0.04
3. $\pi^-p \to E(1420)\tilde{X}$ $K^0K^{*0} \to K^0K^\pm\pi^\mp$ (158 ± 98)	0.60 ± 0.38
4. $\pi^-p \to E(1420)\tilde{X}$ $K^{*\pm}K^\mp \to K^0K^\mp\pi^\pm$ (193 ± 29)	0.74 ± 0.11
5. $\pi^-p \to K^0\phi \to K^0K^+K^-(1840)$ (9 ± 3)	0.05 ± 0.02
6. $\pi^-p \to (A_2K)^0 \to K^0K^+K^-(2003)$ (112 ± 11)	0.26 ± 0.03

VI. CONCLUSIONS

We would like to conclude with some comments on the technique we have used. Nearly all previous spectroscopy experiments have been conducted at comparatively low incident energy. The main reason for this is simply that exclusive se cross sections (for all but the diffractively produced A_1, Q mesons, etc.) such as

$$\pi^-p \to D^0n,$$

fall with increasing energy. (Theoretically for this case, which is A_2 exchange in the Regge picture, it should fall like $1/p_{\text{lab}}$, although the experimental data suggest a faster behavior.) Using experimental low-energy cross sections and theoretical (SU_3) estimates,[15] one soon concludes that the high-energy production cross sections for "interesting" mesons in exclusive channels are too small for useful results in an apparatus such as ours. Resonance production in fully inclusive reactions

$$\pi^-p \to M^*X$$

will be (approximately) energy independent but the additional uninteresting particles in the rest of the final state (i.e., X) lead to large combinatorial backgrounds. For this reason, we choose a compromise semi-inclusive trigger (described in Sec. II) that preserves many (but not all) of the advantages of exclusive reactions but has a much higher cross section. Compared to low-energy data, our experiment is more sensitive for high-mass resonances as the kinematic suppression will be much reduced for us.

We regard our observation of the D and E mesons—the first in any high-energy experiment—as an important test of the technique and an encouraging indication that our methods could make useful contributions to meson spectroscopy. Our $KK\bar{K}$ results are a glimpse of the possible physics that can be probed by future experiments of this type.

Results were presented from the study of multikaon final states in the reactions $\pi^-p \to K^0K^\pm\pi^\mp\tilde{X}$, $K^0K^+K^-\tilde{X}$ at 50 and 100 GeV/c. Here $\tilde{X}$ is semi-inclusive and is only a fraction of a true inclusive event. In the $KK\pi$ final state, the D and E mesons are observed with the following masses, widths, and cross sections times branching ratios (at 100 GeV/c):

$$M_D = 1275 \pm 6 \text{ MeV}, \ \Gamma_D = 22 \pm 21 \text{ MeV}, \ \sigma_D \times B = 0.27 \pm 0.06 \ \mu\text{b} \ [\delta(\delta \to K\bar{K})\pi \text{ mode}]$$

$$M_E = 1440 \pm 5 \text{ MeV}, \ \Gamma_E = 62 \pm 14 \text{ MeV}, \ \sigma_E \times B = 0.63 \pm 0.06 \ \mu\text{b} \ [\delta(\delta \to K\bar{K})\pi \text{ mode}],$$

$$= 0.90 \pm 0.57 \ \mu\text{b} \ (K^{*0}K^0 \text{ mode}),$$

$$= 1.11 \pm 0.16 \ \mu\text{b} \ (K^{*\pm}K^\mp \text{ mode}).$$

The cross section times branching ratio from Table V has been multiplied by 1.5 to include the unseen modes for δ and K^* decay.

The low-statistics three-kaon results presented here indicate two possible mass enhancements. The first state, which decays via the $K^0\phi$ mode, is consistent with being the charmed D^0. Its width (35 ± 30 MeV) agrees with the resolution of the spectrometer for this final state. Its cross section times branching ratio of 0.05 ± 0.02 μb compares favorably (see Sec. IV) with those of charmed baryons and mesons produced in other hadronic reactions. The $K^*\pi$ decay mode (suggested by Fig. 17) has been examined. We find that the data are consistent with this mode but there is no statistically significant effect. The second enhancement, a K^* state, ($M = 2003 \pm 14$ MeV, $W = 87 \pm 43$ MeV) decays into KA_2 and has a cross section times branching ratio of 12 ± 2 μb. This cross section times branching ratio is the average value of K^* and $\bar{K}^*$ at 100 GeV/c. It is obtained by taking the cross section times branching ratio for the $K^0A_2^0$ ($A_2 \to K^+K^-$) mode dividing by both the relevant Clebsch-Gordan coefficient ($\frac{1}{6}$) and the A_2 branching fraction $[(A_2 \to K\bar{K})/(A_2 \to \text{all}) = 0.047 \pm 0.005]$.[1]

ACKNOWLEDGMENTS

We would like to thank F. J. Nagy for furnishing the resonance plus background fitting routines and for valuable discussions concerning their use. We also thank P. Schlein for providing the Čerenkov counters used in this experiment. This work was supported in part by the U.S. Department of Energy under Contracts Nos. DE-AC-03-79-79ER 0068 (Caltech) and DE-AS02-76-EY-02009 (Indiana), and the National Science Foundation under Grant No. PHY-78-07452 (Illinois).

---

*Presently at Michigan State University, East Lansing, Michigan.

†Presently at Hughes Aircraft Corporation, Los Angeles, California.

[1]C. Bricman *et al.*, Phys. Lett. 75B, 1 (1978).

[2]M. J. Corden *et al.*, Nucl. Phys. B144, 253 (1978).

[3]C. Dionisi *et al.*, Bergen–CERN–Collége de France–Madrid–Stockholm Collaborations, Report No. CERN/EP 80-1, 1980 (unpublished).

[4]A. Gurtu *et al.*, Nucl. Phys. B151, 181 (1979).

[5]A. Dzierba, E. Malamud, and D. McLeod, report prepared for the Multiparticle Spectrometer Workshop, Fermilab, 1977 (unpublished); E. Malamud, internal report, 1977 (unpublished); E. Malamud, unpublished notes of Lecture 5 in Fermilab Academic Lectures Series, 1976; G. C. Fox, unpublished memos on E110, 260 software, CIT-14-75 (track finding in one view), CIT-16-75 (matching tracks), CIT-25-76 (vertex determination); H. Haggerty, in Proceedings of the Calorimeter Workshop, Fermilab, 1975 (unpublished), p. 251.

[6]W. Danchi, unpublished memo on E110, CIT-56-79 and Bachelor of Science thesis, California Institute of Technology, 1978 (unpublished).

[7]C. Bromberg *et al.*, Nucl. Phys. B134, 189 (1978).

[8]When the likelihood for an event interpreted as containing a kaon is calculated, one must consider the probability of some light being observed when none is expected. This probability is chosen arbitrarily to be e^{-20} (this is only for convenience and does *not* represent a realistic estimate).

[9]J. O. Dickey, unpublished memo on E110, CIT-57-79.

[10]J. O. Dickey, unpublished memo on E110, CIT-58-79.

[11]D. Drijard *et al.*, Phys. Lett. 81B, 250 (1979).

[12]D. Drijard *et al.*, Phys. Lett. 85B, 452 (1979).

[13]K. L. Giboni *et al.*, Phys. Lett. 85B, 437 (1979).

[14]W. Lockman *et al.*, Phys. Lett. 85B, 443 (1979).

[15]G. C. Fox and A. J. G. Hey, Nucl. Phys. B56, 386 (1973).